Topological quantum pumping in spin-dependent superlattices with glide symmetry

Qianqian Chen, Jianming Cai, and Shaoliang Zhang*
School of Physics, Huazhong University of Science and Technology, Wuhan 430074, China
and International Joint Laboratory on Quantum Sensing and Quantum Metrology,
Huazhong University of Science and Technology, Wuhan 430074, China

(Received 17 September 2019; revised manuscript received 11 March 2020; accepted 12 March 2020; published 20 April 2020)

Topological quantum pumping, also known as topological charge pumping, represents an important quantum phenomenon that shows the fundamental connection to the topological properties of dynamical systems. Here we introduce a pumping process in a spin-dependent double-well optical lattice with glide symmetry. In the dynamic process, the glide symmetry protects the band-touching points, and topological properties of the system are characterized by the non-Abelian Berry curvature. By engineering a suitable form of coupling between different spin components, the model not only demonstrates topological phase transition but also shows hybridization between the spatial and temporal domain with topological features captured by the Wilson line along the synthetic directions. Our work provides a model based on ultracold atoms towards the implementation of versatile topological matters and topological phenomena in condensed matter systems.

DOI: 10.1103/PhysRevA.101.043614

I. INTRODUCTION

Topological quantum pumping [1], also known as the dynamical quantum Hall effect, is a very robust transport process of particles through an adiabatic periodic evolution of the underlying Hamiltonian. In contrast to its classical counterpart, the transport in topological quantum pumping is quantized and is not influenced by the perturbation. Such an important quantum phenomenon is connected to the topological feature of an effective two-dimensional (2D) system, in which the temporal domain induces a synthetic dimension that is perpendicular to the direction of the lattice. The pumped particle in one cycle is characterized by the Chern number of this 2D system [2–5].

In condensed matter physics, the topological quantum pumping is not easily observed because of the challenging requirement for flexible Hamiltonian engineering. Ultracold atom systems, with highly controllable properties, provide a perfect platform to observe these topological phenomena [6,7]. The quantum pumping has already been observed experimentally in ultracold atom systems by driving a superlattice adiabatically [8,9]. Furthermore, a striking manifestation of topological quantum pumping, such as spin pumping [10], has also been observed in ultracold atom systems. Recently, topological quantum pumping in an effective four-dimensional system [11,12] was realized in ultracold atom systems with the measurement of the corresponding second Chern number. Despite these exciting developments, the pumping processes in ultracold atom systems with nonsymmorphic symmetry remain largely unexplored yet. Nonsymmorphic symmetry is one of the spatial group symmetries, which are the combinations of point group operations and nonprimitive lattice transitions. It always leads to novel topological phases, such as nodal points or nodal lines which can be protected by the nonsymmorphic symmetry [13–20]. The pumping processes in these systems are expected to lead to novel quantum phenomena because of the interplay between nonsymmorphic symmetry and topological features.

In this work, we construct a one-dimensional (1D) spin-dependent superlattice with band-touching points which are protected by one of the nonsymmorphic symmetries—glide symmetry—which is the combination of the spin flip and half lattice translation. By modulating the coupling amplitude between different spin components periodically in the pumping process, one can observe a topological phase transition from a regime that can be trivially understood by decoupled chains, to a regime where the coupling becomes significant and the low-energy physics is determined by one emergent band. Although the total particle number pumped is still quantized based on the non-Abelian topological properties of this effective 2D system, the particle number of each spin component pumped in one adiabatic driving cycle is not necessarily an integer anymore. More interestingly, with the appropriate form of coupling between different spin components, the system would exhibit glide symmetry along the hybridized direction of the spatial and temporal domains. The period of Wilson line along this direction is twice as much as the original dynamical system. The present proposal is experimentally feasible based on current state-of-art technology and therefore provides a platform to explore the intriguing topological phenomena with nonsymmorphic symmetry in ultracold atom systems.

This paper is organized as follows. In Sec. II we introduce the model and discuss the band structure of the system. The glide-symmetry-protected band-crossing points require non-Abelian Berry curvature to describe the topological properties. In Sec. III we discuss different types of coupling and the corresponding topological phase transition. The influence of

*shaoliang@hust.edu.cn

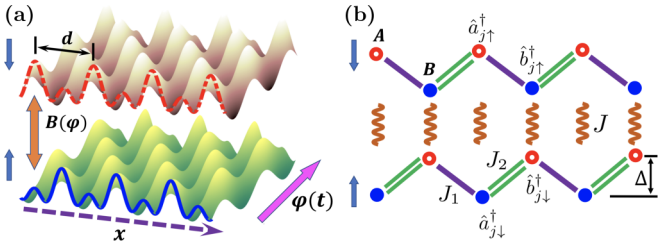

FIG. 1. (a) The evolution of lattice potentials with different spin components. The lattice potentials of spin-up and -down are shown by upper and lower surfaces, respectively. The dashed red line and solid blue line along the x direction (dashed purple arrow) correspond to the lattice potential at $\varphi = 0$ for spin-up and -down, respectively. Lattice potentials of different spin components are driven with the same way along $\varphi(t)$ direction (solid magenta arrow). A microwave field $B(\varphi)$ provides the coupling between spin-up and -down. (b) Tight-binding model of the 1D superlattice for an arbitrary φ. Hollow red dots and solid blue dots represent different sublattice sites. The intrawell (interwell) tunneling $J_1(J_2)$ is shown by a single purple (double green) line. The on-site coupling J is shown by an orange spiral line. Δ is the energy detuning between different sublattices.

different types of glide symmetry in the pumping process is discussed in Sec. IV. Section V is devoted to our conclusions.

II. MODEL

We consider atoms with two internal pseudospin states loaded in a spin-dependent optical lattice. The time-dependent Hamiltonian in the pumping process can be expressed as

$$\mathcal{H}(x,t) = \sum_{\sigma}\int dx\psi_{\sigma}^{\dagger}(x)\left\{-\frac{\hbar^2}{2m}\frac{\partial^2}{\partial x^2} - V_s\cos^2\left(\frac{2\pi x}{d}\right) + V_l\sigma_z\sin\left(\frac{2\pi x}{d}+\varphi\right)\right\}\psi_{\sigma}(x) + \int dx\{B(\varphi)\psi_{\uparrow}^{\dagger}(x)\psi_{\downarrow}(x) + \text{H.c.}\}, \quad (1)$$

gwhere $\sigma = \uparrow, \downarrow$ characterize different hyperfine spin states and $\sigma_z = \pm 1$. V_s and V_l are the lattice depth for lattices with short and long lattice spacing, respectively. The short lattice with $\lambda_s = d/2$ is spin independent, but the long lattice with $\lambda_l = d$ is spin dependent, which means different spin components feel opposite lattice potentials [21–27]. $B(\varphi)$ is the microwave field or Raman lasers coupling different spin components, and the amplitude and phase can be well controlled in experiment [28,29]. The time-dependent parameter $\varphi(t) = \varphi_0 + \omega t$ describes the moving of a spin-dependent lattice along the x direction, where ω is the frequency of the pumping process, which was chosen to make sure the evolution is adiabatic. The evolution of this lattice potential is shown in Fig. 1(a).

In the extreme case $B(\varphi) = 0$, the system can be considered as two independent superlattices. For each spin component, the driving process is equivalent to Thouless pumping, which was already observed in ultracold atom experiments [8,9]. We can explain this equivalence briefly using the tight-binding Hamiltonian as

$$\mathcal{H}(\varphi) = -\sum_n [J_1(\varphi)a_n^{\dagger}b_n + J_2(\varphi)b_n^{\dagger}a_{n+1} + \text{H.c.}] + \frac{\Delta(\varphi)}{2}\sum_n [a_n^{\dagger}a_n - b_n^{\dagger}b_n], \quad (2)$$

where $J_1(\varphi)$ and $J_2(\varphi)$ are the nearest-neighbor tunneling, $\Delta(\varphi)$ is the energy detuning between A and B sublattices, as one of the two chains shown in Fig. 1(b), and all these parameters change periodically with φ. In the adiabatic process, the temporal domain can be regarded as a synthetic dimension perpendicular to the spatial domain and φ as the corresponding quasimomentum; then the time-dependent Hamiltonian (2) can be considered as an effective 2D static Hamiltonian. The Berry curvature in the first Brillouin zone (BZ) and Chern number can be well defined, and one can easily find that the Chern number of the lowest band is $\mathcal{C} = 1$ [30].

If $B(\varphi) \neq 0$, different spin components couple with each other and different quantum phenomena arise. In this case, the total Hamiltonian (1) including two different spin components can also be expressed using tight-binding approximation as

$$\begin{aligned}\mathcal{H} = {} & J_1(\varphi)\sum_n (a_{n,\uparrow}^{\dagger}b_{n,\uparrow} + b_{n,\downarrow}^{\dagger}a_{n+1,\downarrow}) \\ & + J_2(\varphi)\sum_n (b_{n,\uparrow}^{\dagger}a_{n+1,\uparrow} + a_{n,\downarrow}^{\dagger}b_{n,\downarrow}) \\ & + J(\varphi)\sum_n (a_{n,\uparrow}^{\dagger}a_{n,\downarrow} + b_{n,\uparrow}^{\dagger}b_{n,\downarrow}) + \text{H.c.} \\ & + \frac{\Delta(\varphi)}{2}\sum_n (a_{n,\uparrow}^{\dagger}a_{n,\uparrow} - b_{n,\uparrow}^{\dagger}b_{n,\uparrow} \\ & - a_{n,\downarrow}^{\dagger}a_{n,\downarrow} + b_{n,\downarrow}^{\dagger}b_{n,\downarrow}),\end{aligned} \quad (3)$$

where $J(\varphi)$ is the coupling between different spin components which is proportional to $B(\varphi)$. One can also calculate the band structure and other physical properties of this effective 2D system.

With any form of the coupling strength $J(\varphi)$, the band-touching point emerges at the edge of the BZ where $k = \pm\pi/d$ for an arbitrary φ, as shown in Fig. 2. Because of the degeneracy, the non-Abelian Berry curvature is required to describe the topological properties of this effective 2D system. The matrix form of the non-Abelian Berry curvature is [31,32]

$$\boldsymbol{\mathcal{F}} = \partial_k\boldsymbol{\mathcal{A}}_{\varphi} - \partial_{\varphi}\boldsymbol{\mathcal{A}}_k - i[\boldsymbol{\mathcal{A}}_k, \boldsymbol{\mathcal{A}}_{\varphi}], \quad (4)$$

where $\boldsymbol{\mathcal{A}}_k = i\langle\mathbf{u}|(\partial/\partial k)|\mathbf{u}\rangle$ and $\boldsymbol{\mathcal{A}}_{\varphi} = i\langle\mathbf{u}|(\partial/\partial\varphi)|\mathbf{u}\rangle$ are Berry-Wilzeck-Zee connections [33,34], which are both 2×2 matrix where $|\mathbf{u}\rangle = \{|u_n(k,\varphi)\rangle\}$ $(n \leqslant 2)$ is the instantaneous periodic Bloch wave function of the lowest two bands at an arbitrary φ [where $|\psi_n(k,\varphi)\rangle = e^{ikx}|u_n(k,\varphi)\rangle$ is the corresponding Bloch wave function]. The particle number transported within one cycle can be characterized with the non-Abelian Chern number [35–37]

$$Q = -\frac{1}{2\pi}\int_0^{2\pi}\int_{\text{BZ}}\text{tr}(\boldsymbol{\mathcal{F}})\,dk\,d\varphi. \quad (5)$$

It means that the pumped particles in each cycle should also be quantized. We should point out this conclusion is relevant only

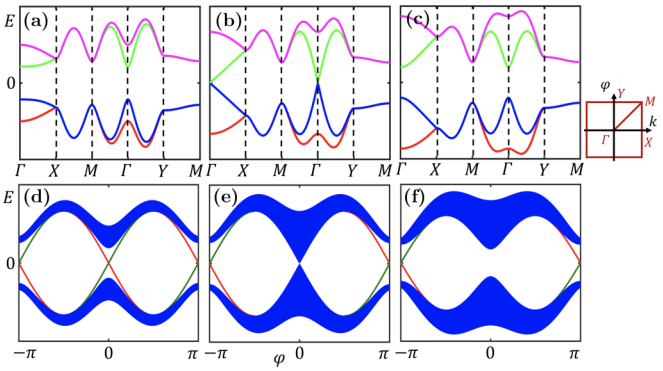

FIG. 2. (a)–(c). Band structure of the effective 2D system in different topological phases, where the coupling has the form as $J(\varphi) = J(1+\cos\varphi)$. (a) $J < (J_1+J_2)/2$, (b) $J = (J_1+J_2)/2$, (c) $J > (J_1+J_2)/2$. (d)–(f) The corresponding energy spectrum for different φ in a 1D superlattice with an open boundary condition. (d) When $J < (J_1+J_2)/2$, there are two zero energy modes at $\varphi = 0$ and π, respectively. (e) When $J = (J_1+J_2)/2$, there is a band-touching point at $\varphi = 0$, and the topological phase transition occurs. (f) When $J > (J_1+J_2)/2$, the band gap reopens, and there is only one zero energy mode at $\varphi = \pi$.

for weakly interacting bosons when the driving frequency ω satisfying the condition $\mathcal{W} \ll \hbar\omega \ll \mathcal{D}$, where $\mathcal{W}$ is the band width of lowest two bands and $\mathcal{D}$ is energy gap between lowest two bands and the other upper bands. Only in this case can the lowest two bands be approximated as degenerate in the whole BZ and the probability of the excitation to the upper bands can be ignored, which means the dynamic process can be considered as an adiabatic evolution in the subspace of lowest two almost degenerate bands. For fermions, the condition $\mathcal{W} \ll \hbar\omega$ is not needed because of the Pauli exclusion principle, but $\hbar\omega \ll \mathcal{D}$ should still be satisfied.

III. TOPOLOGICAL PHASE TRANSITION

In the extreme case $J(\varphi) = 0$, the lowest two bands are degenerate in the whole BZ and the Chern number of the effective 2D system should be $C = 2$. With the increase of the amplitude of the microwave field, the gap will be opened in most of the BZ. But at $k = \pm\pi/d$, the degeneracy will be protected by glide symmetry [38]. With different forms of coupling $J(\varphi)$ corresponding to different types of glide symmetry, different quantum phenomena can be observed. So the form of $J(\varphi)$ is crucial for the non-Abelian topological properties in this effective 2D system. In the following, we will discuss two typical types of coupling and their topological consequences.

Case 1: $J(\varphi)$ is real. In this case, with the combination of a spatial translation of half of the lattice spacing $d/2$ and the spin flip $\uparrow \leftrightarrow \downarrow$, the Hamiltonian (1) is conserved. This operation is independent of φ, which means the spatial and temporal domain is separated, and we can say the system has *spatial glide symmetry*. In a tight-binding approximation, the corresponding spatial glide operator can be written as

$$\hat{G}_k = e^{\frac{ikd}{2}}\left(\cos\frac{kd}{2}\sigma_1\tau_1 + \sin\frac{kd}{2}\sigma_1\tau_2\right), \tag{6}$$

where $\boldsymbol{\sigma}$ and $\boldsymbol{\tau}$ are Pauli matrices describing the hyperfine spin state and pseudospin states on sublattices A and B, respectively. The operator $\hat{G}_k$ satisfies the relation $\hat{G}_k\mathcal{H}_k\hat{G}_k^{-1} = \mathcal{H}_k$ where $\mathcal{H}_k$ is the Fourier transformation of tight-binding Hamiltonian (3), and $\hat{G}_k^2|\psi_{k,n}\rangle = e^{ikd}|\psi_{k,n}\rangle$ as $\hat{G}_k^2$ is a translation for one lattice spacing. The proof of the relation between the emergence of band-touching point on the edge of BZ and the glide symmetry was shown in our earlier work [38]. If $J(\varphi) = 2J$ is a constant, with the increase of the amplitude of the microwave field, the topological phase transition emerges at $2J = J_1 + J_2$ and the Chern number of lowest two bands becomes $C = 0$ when passing across this critical point. But if the amplitude of $J(\varphi)$ has a modulation in the temporal domain, for example, $J(\varphi) = J(1+\cos\varphi)$ where $J > 0$, then the topological phase transition emerges at the same point with the increase of the amplitude, but the Chern number of lowest two bands will become $C = 1$ instead of $C = 0$. In the experiment, the topological phase transition can be directly observed by measuring the movement of center of mass (COM) of the atoms in one cycle. One can prepare the initial state in the Mott-insulator phase with the lowest two bands fully filled. Then the movement of COM should have a sharp transition from one side of the critical point to the other. It means that if the amplitude of coupling is modulated periodically, although the total particle number transported in one cycle is quantized to 1, each spin component transported can have no quantization property in the pumping process.

This topological phase transition can be explained as follows. With an arbitrary φ, the topological properties of the instantaneous 1D Hamiltonian are characterized by the Zak phase. Only two special times $\varphi = 0$ and $\varphi = \pi$ need to be considered, because at these moments, this 1D system is a two-leg Su-Schrieffer-Heeger (SSH) model and the Zak phase should be 0 or π, which depends on the coupling strength $J(\varphi)$, as discussed in our earlier work [38]. Because $J(\varphi) = J(1+\cos\varphi)$ has a modulation in temporal domain, the system touches the critical point only at $\varphi = 0$ when $2J = J_1 + J_2$, as shown in Figs. 2(a)–2(c). If the system has an open boundary condition in real space, the topological phase transition can also be characterized by the change of edge states, as shown in Figs. 2(d)–2(f). Although the conclusions come from the tight-binding model, the numerical calculation with plane-wave expansion can get the same results, which was shown in the Appendix.

Case 2: $J(\varphi)$ is complex, namely, $J(\varphi) = J(1+e^{i\varphi})$. In this case, the glide operation which conserves the Hamiltonian (1) is the combination of a spatial translation of half of the lattice spacing $d/2$ and the spin flip with an φ-dependent phase $\psi_\uparrow(x) \to \psi_\downarrow(x)$, $\psi_\downarrow(x) \to e^{-i\varphi}\psi_\uparrow(x)$. In this case, the spatial and temporal operations couple with each other, leading to the fact that the spatial and temporal domain is inseparable [39]. Therefore, the system demonstrates a type of symmetry, namely, *synthetic glide symmetry*. Using a similar method, the corresponding synthetic glide operator can be written as

$$\hat{G}_{k,\varphi} = e^{\frac{i(kd-\varphi)}{2}}\left(\cos\frac{kd}{2}\cos\frac{\varphi}{2}\sigma_1\tau_1 - \sin\frac{kd}{2}\sin\frac{\varphi}{2}\sigma_2\tau_2 + \sin\frac{kd}{2}\cos\frac{\varphi}{2}\sigma_1\tau_2 - \cos\frac{kd}{2}\sin\frac{\varphi}{2}\sigma_2\tau_1\right), \tag{7}$$

where $\hat{G}^2_{k,\varphi}|\psi_{k,n}\rangle = e^{i(kd-\varphi)}|\psi_{k,n}\rangle$, which is a translation along the synthetic direction instead of a lattice spacing. With the increase of the coupling strength, the system also exhibits a topological phase transition from $C = 2$ to $C = 1$ at the critical point $2J = J_1 + J_2$. It can be seen that the position of critical point depends only on the amplitude of the coupling $|J(\varphi)| = J\sqrt{2(1+\cos\varphi)}$.

IV. WILSON LINE

It looks like the above two cases have similar behaviors in topological phase transition. But we should point out that the topological properties of these two systems are different because of two different types of glide symmetry. In these effective 2D systems, the Wilson line is required to characterize the non-Abelian topological properties [34,40]. For example, the Wilson line starting from $\Gamma = (0, 0)$ pointing to an arbitrary point $\mathbf{k} = (k, \varphi)$ can be defined as

$$\mathcal{W}_{\Gamma\to\mathbf{k}} = \mathscr{P}\exp\left\{i\int_L \boldsymbol{\mathcal{A}}(\mathbf{k})\cdot d\mathbf{k}\right\}, \tag{8}$$

which is a path-ordered ($\mathscr{P}$) integral and L is the path from Γ to $\mathbf{k}$ in reciprocal space. In experiment, if the initial state was prepared on the eigenstate of the nth band as $|\psi_n(0, 0)\rangle$ with quasimomentum $k = 0$, the amplitude of matrix element of a Wilson line can be estimated by detecting the population of atoms on the mth band at quasimomentum $\mathbf{k}$ after the dynamic evolution along route L as $|W^{mn}_{\Gamma\to\mathbf{k}}|^2$ where

$$W^{mn}_{\Gamma\to\mathbf{k}} = \langle u_m(k,\varphi)|\mathcal{W}_{\Gamma\to\mathbf{k}}|u_n(0,0)\rangle. \tag{9}$$

The measurement of phases of the Wilson line is also possible in ultracold atoms [41]. But in our work, it is not needed because only the measurement of the amplitude can distinguish the influence of different glide symmetries. To ensure the above relation (9) is correct, the criterion $\mathcal{W} \ll \hbar\omega \ll \mathcal{D}$ should also be satisfied due to the same reason in the discussion of Eq. (5). Because the amplitude of $J(\varphi)$ determines the topological phases, both $\mathcal{W}$ and $\mathcal{D}$ are related to J. When J is much smaller than the other energy scales, the band width $\mathcal{W}$ is approximately equal to $2J$, so the driven frequency ω should be larger than J. However, after passing the critical point, the increase of J only enlarges the band gap $\mathcal{D}$ where $\mathcal{W}$ depends on other energy scales, so ω should be much smaller than J. The Wilson line can be expressed as a sequence of path-ordered products of projectors and calculated numerically [42–44].

In the spatial-temporal separable system, because $\langle u_1(k,\varphi)|\partial_\varphi|u_2(k,\varphi)\rangle = 0$, which means the eigenstates of the lowest two bands cannot couple with each other in a pumping process, the Wilson line is a trivial straight line. But in the spatial-temporal inseparable system, because of the hybridization of the spatial and temporal domains, $\langle u_1(k,\varphi)|\partial_\varphi|u_2(k,\varphi)\rangle \neq 0$, and the tunneling between different bands will be induced in the pumping process. The form of the Wilson line will always be complex and depends on the route of adiabatic evolution. In Fig. 3(b) the route of evolution is only in the temporal domain and the quasimomentum is $k = 0$, as the solid magenta arrow shows in Fig. 3(a). The population on the ground state decreases smoothly from 1 but increases suddenly after going through the edge of the BZ. The Wilson line has the same period as the original Hamiltonian in the temporal domain. In Fig. 3(c) we add a very small force to accelerate the atoms in the spatial domain and drive the system in the temporal domain simultaneously. By fine-tuning the force as $F = \hbar\dot{k} = \hbar\omega/d$, one can control the atoms moving along the diagonal line of the BZ of this effective 2D system, as the dashed green arrow shows in Fig. 3(a). After one period of driving, the state flips to the eigenstate of the first excited band, which is orthogonal to the initial state. Only after another period can it return to the initial one, which corresponds to a Möbius strip.

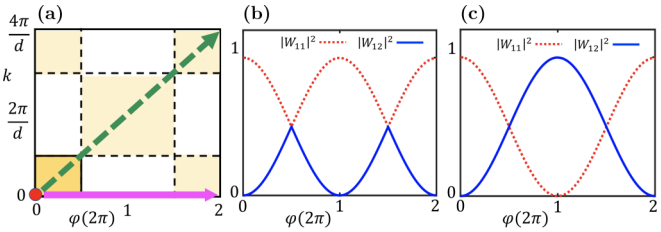

FIG. 3. Wilson line. The initial state was prepared on the ground state at $k = 0$. (a) The solid magenta and dashed green arrows correspond to two pumping processes along different directions respectively. The yellow area is part of the first BZ. The white and light yellow areas correspond to the ground states that have "+" and "−" eigenvalues of the glide operator respectively. (b) and (c) The population on different bands in the pumping process along different directions. Panel (b) is along the φ direction and keeps $k = 0$, and panel (c) is along the diagonal line of the first BZ as $\varphi = kd$. The parameters are $V_s = 8E_R$, $V_l = 4E_R$ and $B_0 = 0.01E_R$, where $E_R = \hbar^2\pi^2/(2md^2)$ is the recoil energy.

All these results arise from the synthetic glide symmetry. In the extreme case that the coupling amplitude approaches zero, the lowest two bands are almost degenerate in the whole BZ and the Wilson line can be calculated analytically. If the pumping is along φ direction as the solid magenta arrow shows in Fig. 3(a), the Wilson line has the matrix form as

$$W_{0\to\varphi} = e^{i\theta(\varphi)}\begin{pmatrix}\cos(\varphi/4) & -i\sin(\varphi/4)\\ -i\sin(\varphi/4) & \cos(\varphi/4)\end{pmatrix}, \tag{10}$$

where the bases are the lowest two eigenstates of instantaneous Hamiltonian $|u^-_{k\varphi}(x)\rangle$ and $|u^+_{k\varphi}(x)\rangle$, and $\pm$ corresponds to different eigenvalues of glide symmetry operator, respectively. Here $e^{i\theta(\varphi)}$ is the U(1) part with a complex form, and the SU(2) part shows that the populations on "−" and "+" bands in evolution should be $|W_{--}|^2 = \cos^2(\varphi/4) = [1 + \cos(\varphi/2)]/2$ and $|W_{-+}|^2 = \cos^2(\varphi/4) = [1 - \cos(\varphi/2)]/2$, which have a period of 4π in the temporal domain if the initial state is prepared on the ground state $|u^-_{k\varphi}(x)\rangle$. But in this pumping process, there is a band-crossing point at the edge of BZ where $\varphi = \pi$ because of the synthetic glide symmetry, and after passing this point, $|u^+_{k\varphi}(x)\rangle$ becomes the ground state. So the population on the lowest band $|W_{11}|^2$ should flip from $|W_{--}|^2$ to $|W_{-+}|^2$, and it will flip again after passing another edge. The period of the population evolution is 2π as shown in Fig. 3(b). If the pumping is along the diagonal direction of BZ as the dashed green arrow shows in Fig. 3(a), the matrix form of the Wilson line is similar to Eq. (10), except that φ is replaced by the parameter

$p = (kd + \varphi)/2$ along the hybridized direction, but $|u^{-}_{k\varphi}(x)\rangle$ is always the ground state along this direction because of the synthetic glide symmetry. Then the population on the lowest band should always be $|W_{--}|^2$, and the period of evolution is 4π as shown in Fig. 3(c). We point out that all the evolution of the population on the ground state can be directly measured in experiment if the initial state prepared in the superfluid phase instead of the Mott-insulator phase. More analytical proof and detailed discussions are shown in the Appendix.

V. CONCLUSION

In this work, we propose a quantum pumping process by periodically driving a spin-dependent superlattice. Because of the glide symmetry, the band structure has nodal lines, and the topological properties of this system should be characterized by non-Abelian Berry curvature. In this system, we find that the topological phase transition can be well controlled by the form of coupling between different spin components. Especially, we can find the case that each spin component transported in one cycle is not quantized in our system, although the total particle number pumped is still quantized. In addition, the interplay between the glide symmetry and the coupling between different spin components can hybridize the temporal and spatial domains, which induces the synthetic glide symmetry, and may open a route to topological phenomena, such as a Möbius strip without the need of a twisted boundary. The spin-dependent superlattice system can be highly controlled experimentally and exhibit versatile physics. The generalization of the present model allows realizing the Floquet topological systems with nonsymmorphic symmetry using a periodically driving process with high frequency [39,45–48]. The influence of interaction on topological pumping processes may open up more interesting quantum phenomena.

ACKNOWLEDGMENTS

We acknowledge the useful discussion with Xiang-Fa Zhou, and S.L.Z. also thanks Qi Zhou and Zheng-Wei Zhou for valuable suggestions. S.L.Z. was supported by start-up funding of Huazhong University of Science and Technology. J.M.C. was supported by the National Key R&D Program of China (Grant No. 2018YFA0306600).

APPENDIX A: THE RESULT OF TOPOLOGICAL PROPERTY OF THE QUANTUM PUMPING PROCESS WITH EXACT CALCULATION USING PLANE-WAVE EXPANSION

Using the plane-wave expansion, we check all results in the main text and find consistent results. We chose two types of interspin coupling where the spatial and temporal domains are separable and inseparable, respectively.

Consider the spatial-temporal separable system first. To generalize our results, the microwave field coupling different spin components should have the form $B(\varphi) = B_0(1 + \cos\varphi)$ The band structure is shown in Fig. 4. One can see that the band structure of this effective 2D system using plane-wave expansion is similar to that deduced from the tight-binding model in the main text with only quantitative differences. The asymmetry of the lower and upper two bands mainly comes

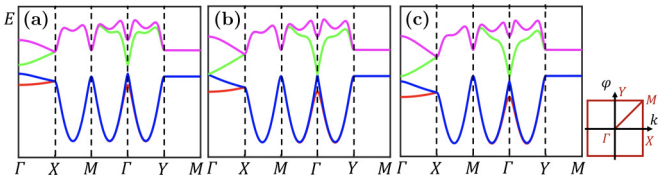

FIG. 4. Band structure of the effective two-dimensional system with coupling $B(\varphi) = B_0(1 + \cos\varphi)$ using plane-wave expansion. The lattice depths with short and long wavelength are $V_s = V_l = 6E_R$ respectively. (a) $B_0 = 0.5E_R$, (b) $B_0 = 0.8E_R$, (c) $B_0 = 1.0E_R$.

from the next-nearest-neighbor tunneling and the influence of the higher bands. Here we choose the lattice depth with short and long wavelength to be $V_s = V_l = 6E_R$ where $E_R = \frac{h^2}{2md^2}$ is the recoil energy. One can easily check that the topological properties are similar to the result of tight-binding model. When $B_0 \approx 0.8E_R$, this effective 2D system has a band-touching point at Γ point and thus has a topological phase transition, as shown in Fig. 4(b). Figure 5 shows the trace of non-Abelian Berry curvature on two sides of this topological phase transition.

Then we consider the spatial-temporal inseparable system. In this case, the microwave field coupling different spin components should have the form $B(\varphi) = B_0(1 + e^{i\varphi})$ to preserve the synthetic glide symmetry. The band structure is almost same as Fig. 4, and the topological phase transition can also be observed.

APPENDIX B: DISCUSSION ABOUT THE WILSON LINE

Consider the extreme case $B(\varphi) = 0$ first. The Hamiltonian of each spin component is

$$\mathcal{H}_\sigma(x,\varphi) = \int dx \psi^\dagger_\sigma(x)\left\{-\frac{\hbar^2}{2m}\frac{\partial^2}{\partial x^2} - V_s\cos^2\left(\frac{2\pi x}{d}\right) + V_l\sigma_z\sin\left(\frac{2\pi x}{d} + \varphi\right)\right\}\psi_\sigma(x), \tag{B1}$$

which has the relation as $\mathcal{H}_\uparrow(x,\varphi) = \mathcal{H}_\downarrow(x + d/2, \varphi)$. Assume that the plane-wave solution of the Bloch wave function on the lowest bands of the instantaneous Hamiltonian

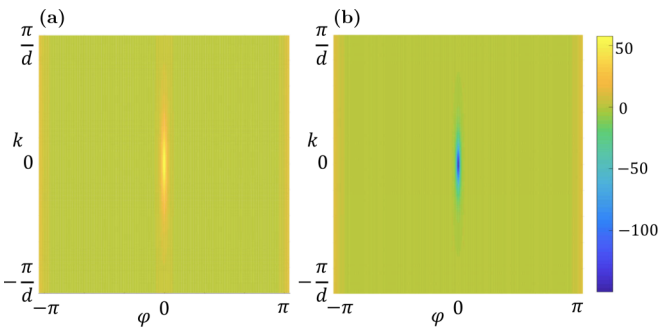

FIG. 5. The trace of non-Abelian Berry curvature of the effective two-dimensional system in different topological phases. The lattice depth with short and long wavelength are $V_s = V_l = 6E_R$ respectively. (a) $B_0 = 0.5E_R$, (b) $B_0 = 1.0E_R$.

$\mathcal{H}_\uparrow(x,\varphi)$ is

$$\begin{aligned}|\psi_{k\varphi,\uparrow}(x)\rangle =& e^{ikx}|u_{k\varphi,\uparrow}(x)\rangle \\ =& \frac{e^{ikx}}{\sqrt{d}}\sum_\ell c_\ell(k,\varphi)\exp\left\{\frac{i2\pi\ell x}{d}\right\}|\uparrow\rangle,\end{aligned} \tag{B2}$$

which has the eigenenergy $\epsilon(k,\varphi)$. We have the relation $\sum_\ell |c_\ell(k,\varphi)|^2 = 1$ because of the normalization of the Bloch wave function. Then the corresponding plane-wave solution of the instantaneous Hamiltonian $\mathcal{H}_\downarrow(x,\varphi)$ with the same eigenenergy should have the form as

$$\begin{aligned}|\psi_{k\varphi,\downarrow}(x)\rangle =& e^{ikx}|u_{k\varphi,\downarrow}(x)\rangle \\ =& \frac{e^{ikx}}{\sqrt{d}}\sum_\ell (-1)^\ell c_\ell(k,\varphi)\exp\left\{\frac{i2\pi\ell x}{d}\right\}|\downarrow\rangle,\end{aligned} \tag{B3}$$

which satisfy the relation $\psi_{k\varphi,\uparrow}(x) = \psi_{k\varphi,\downarrow}(x+d/2)$. Then we consider the case that $B(\varphi)$ is not zero, where different spin components and different energy bands with the same quasimomentum k will be coupled and the result will be very complex. But if the coupling strength is very small, only the subspace spanned by the lowest band needs to be considered. Then the effective Hamiltonian can be written as a 2D matrix using these two states as bases. The diagonal term is identical, and the off-diagonal term is the coupling between two spin components, which can be estimated as $\Omega_{k,\varphi}B(\varphi)$ where

$$\begin{aligned}\Omega_{k,\varphi} =& \int_0^d \psi^*_{k\varphi,\downarrow}(x)\psi_{k\varphi,\uparrow}(x)\,dx \\ =& \sum_\ell (-1)^\ell |c_\ell(k,\varphi)|^2.\end{aligned} \tag{B4}$$

It can be validated numerically that $\Omega_{k,\varphi}$ is always positive in the first BZ. Then we need to discuss two different cases that $B(\varphi)$ is real and complex separately.

1. The spatial and temporal domain are separable

Assume that the coupling has the form $B(\varphi) = B_0(1+\cos\varphi)$, then the effective Hamiltonian can be written as

$$\mathcal{H}_{\rm eff}(k,\varphi) = \epsilon_{k,\varphi}\mathcal{I} + B_0(1+\cos\varphi)\Omega_{k,\varphi}\sigma_x. \tag{B5}$$

The eigenstates of this effective Hamiltonian can be written as

$$\begin{aligned}|\psi^\pm_{k,\varphi}(x)\rangle =& \{|\psi_{k\varphi,\uparrow}(x)\rangle \pm |\psi_{k\varphi,\downarrow}(x)\rangle\}/\sqrt{2} \\ =& \frac{e^{ikx}}{\sqrt{2d}}\sum_\ell c_\ell(k,\varphi)\exp\left\{\frac{i2\pi\ell x}{d}\right\} \\ & \times(|\uparrow\rangle \pm (-1)^\ell|\downarrow\rangle).\end{aligned} \tag{B6}$$

The sign of the ground state depends only on the sign of coupling $B_0 + B'\cos(\varphi)$. For example, if $B_0 > B' > 0$, it is always positive, which means $|\psi^-_{k,\varphi}(x)\rangle$ is always the ground state. The form of the non-Abelian Berry connection can be estimated as

$$\begin{aligned}i\langle u^+_{k\varphi}(x)|\partial_\varphi|u^+_{k\varphi}(x)\rangle =& i\langle u^-_{k\varphi}(x)|\partial_\varphi|u^-_{k\varphi}(x)\rangle \\ =& i\sum_\ell c^*_\ell(k,\varphi)\partial_\varphi c_\ell(k,\varphi), \\ i\langle u^+_{k\varphi}(x)|\partial_\varphi|u^-_{k\varphi}(x)\rangle =& 0,\end{aligned} \tag{B7}$$

which has only the diagonal term. From the Eq. (6), we know that the form of the Wilson line in this case is a straight line; there is no population transition in the pumping process.

2. The spatial and temporal domain are inseparable

When the coupling has the form $B(\varphi) = B_0(1+e^{i\varphi})$, the result will be very different. In this case, the coupling is complex, so the effective Hamiltonian has a different form as

$$\begin{aligned}\mathcal{H}_{\rm eff}(k,\varphi) =& \epsilon_{k,\varphi}\mathcal{I} + B_0(1+\cos\varphi)\Omega_{k,\varphi}\sigma_x \\ & - B_0\sin\varphi\Omega_{k,\varphi}\sigma_y.\end{aligned} \tag{B8}$$

Because the off-diagonal terms can be rewritten as $2B_0\cos(\varphi/2)e^{i\varphi/2}\Omega_{k,\varphi}$, which has an additional phase $e^{i\varphi/2}$, the eigenstates of the effective Hamiltonian are

$$\begin{aligned}|\psi^\pm_{k,\varphi}(x)\rangle =& \{|\psi_{k\varphi,\uparrow}(x)\rangle \pm e^{-i\varphi/2}|\psi_{k\varphi,\downarrow}(x)\rangle\}/\sqrt{2} \\ =& \frac{e^{ikx}}{\sqrt{2d}}\sum_\ell c_\ell(k,\varphi)\exp\left\{\frac{i2\pi\ell x}{d}\right\} \\ & \times(|\uparrow\rangle \pm (-1)^\ell e^{-i\varphi/2}|\downarrow\rangle).\end{aligned} \tag{B9}$$

Then if the pumping process is in the temporal domain, the matrix elements of the non-Abelian Berry connection is

$$\begin{aligned}i\langle u^+_{k\varphi}(x)|\partial_\varphi|u^+_{k\varphi}(x)\rangle =& i\langle u^-_{k\varphi}(x)|\partial_\varphi|u^-_{k\varphi}(x)\rangle \\ =& i\sum_\ell c^*_\ell(k,\varphi)\partial_\varphi c_\ell(k,\varphi) + \frac{1}{4}, \\ i\langle u^+_{k\varphi}(x)|\partial_\varphi|u^-_{k\varphi}(x)\rangle =& i\langle u^-_{k\varphi}(x)|\partial_\varphi|u^+_{k\varphi}(x)\rangle = -\frac{1}{4}.\end{aligned} \tag{B10}$$

Because $\alpha_k(\varphi) = i\sum_\ell c^*_\ell(k,\varphi)\partial_\varphi c_\ell(k,\varphi)$ is a real number, the form of the Wilson line can be estimated as

$$\begin{aligned}\mathcal{W}_{0\to\varphi} =& \exp\left\{\mathcal{T}\int_0^\varphi i\boldsymbol{\mathcal{A}}(\varphi)d\varphi\right\} \\ =& \exp\left\{\mathcal{T}\int_0^\varphi i\left[\left(\alpha_k+\frac{1}{4}\right)\mathcal{I} - \frac{1}{4}\sigma_x\right]d\varphi\right\} \\ =& e^{i\theta(\varphi)}\exp\left\{-\frac{i}{4}\int_0^\varphi \sigma_x d\varphi\right\} \\ =& e^{i\theta(\varphi)}\begin{pmatrix}\cos(\varphi/4) & -i\sin(\varphi/4) \\ -i\sin(\varphi/4) & \cos(\varphi/4)\end{pmatrix},\end{aligned} \tag{B11}$$

where $\theta(\varphi) = \int_0^\varphi(\alpha_k + 1/4)d\varphi$ is the global phase. If the initial state is prepared on the ground state $|\psi^-_{k,\varphi}(x)\rangle$, the populations of different bands in the pumping process should be

$$\begin{aligned}|W_{--}|^2 =& \cos^2\frac{\varphi}{4} = \frac{1}{2}\left(1+\cos\frac{\varphi}{2}\right), \\ |W_{-+}|^2 =& \sin^2\frac{\varphi}{4} = \frac{1}{2}\left(1-\cos\frac{\varphi}{2}\right),\end{aligned} \tag{B12}$$

which have a period of 4π. Because of the glide operation along the synthetic dimension where $|\uparrow\rangle \to |\downarrow\rangle$ and $|\downarrow\rangle \to e^{i\varphi}|\uparrow\rangle$, $|\psi^\pm_{k,\varphi}(x)\rangle$ are the eigenstates of this synthetic

glide operator with eigenvalues "+" and "−," respectively. But we should point out that the amplitude of coupling $2B_0\cos(\varphi/2)\Omega_{k,\varphi}$ will change the sign after passing the edge of the first BZ; it means that in the range of $\pi \leqslant \varphi \leqslant 3\pi$, $|\psi^{+}_{k,\varphi}(x)\rangle$ will be the ground state, and the population on the ground state should changes from $|W_{--}|^2$ to $|W_{-+}|^2$. That is the reason we can get the result in Fig. 3(b) [38].

If the pumping process is along the diagonal direction of the BZ of the effective Hamiltonian, we should redefine new parameters $p = (kd + \varphi)/2$ and $q = (kd - \varphi)/2$. The inverse transformation is $kd = p + q$ and $\varphi = p - q$. The eigenstates can be described using new coordinates as

$$|u^{\pm}_{pq}(x)\rangle = \frac{1}{\sqrt{2d}}\sum_{\ell} c_\ell(p,q)e^{2\pi i\ell x/d} \times \{|\uparrow\rangle \pm (-1)^{\ell}e^{i(q-p)/2}|\downarrow\rangle\}. \quad \text{(B13)}$$

One can also estimate all elements of the non-Abelian Berry connection along the p direction using a similar method, and the form of the Wilson line is the same as Eq. (B11). But in this case, the difference is that the eigenstates $|u_{pq,+}(x)\rangle$ and $|u_{pq,-}(x)\rangle$ will not flip when crossing the edge of the first BZ, since, although $2B_0\cos(\varphi/2)$ flips the sign, the quasimomentum k also goes through the edge of BZ, which results in $\Omega_{k,\varphi} = \sum_\ell(-1)^\ell|c_\ell(k,\varphi)|^2$ flipping the sign as well. This result comes from the properties of Bloch wave function that $c_\ell(k + 2\pi/d) = c_{\ell+1}(k)$. So the coupling amplitude $2B_0\cos(\varphi/2)\Omega_{k,\varphi}$ will not change the sign, and the population on the lowest band will always be $|W_{--}|^2$ as shown in Eq. (B12), which leads to the result in Fig. 3(c).

With the increase of the coupling amplitude $\Omega(\varphi)$, the influence of higher bands of Hamiltonian $\mathcal{H}_\sigma(x,\varphi)$ such as the p band cannot be ignored. The lowest four bands need to be considered, and there is no analytical result in this case. With numerical calculation, one can find that the dominant population on the lowest two bands should be $|\psi^{s,-}\rangle$ and $|\psi^{p,-}\rangle$ instead of $|\psi^{s,+}\rangle$ and $|\psi^{s,+}\rangle$ after passing the critical point of the topological phase transition. But the qualitative properties of Wilson loop along two different routes still remain unchanged.

[1] D. J. Thouless, Quantization of particle transport, Phys. Rev. B **27**, 6083 (1983).

[2] M. J. Rice and E. J. Mele, Elementary Excitations of a Linearly Conjugated Diatomic Polymer, Phys. Rev. Lett. **49**, 1455 (1982).

[3] R. D. King-Smith and D. Vanderbilt, Theory of polarization of crystalline solids, Phys. Rev. B **47**, 1651 (1993).

[4] L. Fu and C. L. Kane, Time reversal polarization and a Z_2 adiabatic spin pump, Phys. Rev. B **74**, 195312 (2006).

[5] R. Citro, A topological charge pump, Nat. Phys. **12**, 288 (2016).

[6] V. Galitski and I. B. Spielman, Spin-orbit coupling in quantum gases, Nature (London) **494**, 49 (2013).

[7] I. B. Spielman, Detection of topological matter with quantum gases, Ann. Phys. **525**, 797 (2013).

[8] M. Lohse, C. Schweizer, O. Zilberberg, M. Aidelsburger, and I. Bloch, A Thouless quantum pump with ultracold bosonic atoms in an optical superlattice, Nat. Phys. **12**, 350 (2016).

[9] S. Nakajima, T. Tomita, S. Taie, T. Ichinose, H. Ozawa, L. Wang, M. Troyer, and Y. Takahashi, Topological Thouless pumping of ultracold fermions, Nat. Phys. **12**, 296 (2016).

[10] C. Schweizer, M. Lohse, R. Citro, and I. Bloch, Spin Pumping and Measurement of Spin Currents in Optical Superlattices, Phys. Rev. Lett. **117**, 170405 (2016).

[11] M. Lohse, C. Schweizer, H. M. Price, O. Zilberberg, and I. Bloch, Exploring 4D quantum Hall physics with a 2D topological charge pump, Nature (London) **553**, 55 (2018).

[12] O. Zilberberg, S. Huang, J. Guglielmon, M. Wang, K. P. Chen, Y. E. Kraus, and M. C. Rechtsman, Photonic topological boundary pumping as a probe of 4D quantum Hall physics, Nature (London) **553**, 59 (2018).

[13] S. M. Young and C. L. Kane, Dirac Semimetals in Two Dimensions, Phys. Rev. Lett. **115**, 126803 (2015).

[14] C. Fang and L. Fu, New classes of three-dimensional topological crystalline insulators: Nonsymmorphic and magnetic, Phys. Rev. B **91**, 161105(R) (2015)

[15] B. Bradlyn, J. Cano, Z. Wang, M. G. Vergniory, C. Felser, R. J. Cava, and B. A. Bernevig, Beyond Dirac and Weyl fermions: Unconventional quasiparticles in conventional crystals, Science **353**, aaf5037 (2016).

[16] A. Alexandradinata, Z. Wang, and B. A. Bernevig, Topological Insulators from Group Cohomology, Phys. Rev. X **6**, 021008 (2016).

[17] T. Bzduek, Q. Wu, A. Regg, M. Sigrist, and A. A. Soluyanov, Nodal-chain metals, Nature (London) **538**, 75 (2016).

[18] J. Kruthoff, J. de Boer, J. van Wezel, C. L. Kane, and R.-J. Slager, Topological Classification of Crystalline Insulators through Band Structure Combinatorics, Phys. Rev. X **7**, 041069 (2017).

[19] B. J. Wieder, B. Bradlyn, Z. Wang, J. Cano, Y. Kim, H.-S. D. Kim, A. M. Rappe, C. L. Kane, and B. A. Bernevig, Wallpaper fermions and the nonsymmorphic Dirac insulator, Science **361**, 246 (2018).

[20] F. Zhang and C. L. Kane, Anomalous topological pumps and fractional Josephson effects, Phys. Rev. B **90**, 020501(R) (2014).

[21] V. Finkelstein, P. R. Berman, and J. Guo, One-dimensional laser cooling below the Doppler limit, Phys. Rev. A **45**, 1829 (1992).

[22] I. H. Deutsch and P. S. Jessen, Quantum-state control in optical lattices, Phys. Rev. A **57**, 1972 (1998).

[23] D. L. Haycock, P. M. Alsing, I. H. Deutsch, J. Grondalski, and P. S. Jessen, Mesoscopic Quantum Coherence in an Optical Lattice, Phys. Rev. Lett. **85**, 3365 (2000).

[24] O. Mandel, M. Greiner, A. Widera, T. Rom, T. W. Hänsch, and I. Bloch, Coherent Transport of Neutral Atoms in Spin-Dependent Optical Lattice Potentials, Phys. Rev. Lett. **91**, 010407 (2003).

[25] D. McKay and B. DeMarco, Thermometry with spin-dependent lattices, New J. Phys. **12**, 055013 (2010).

[26] P. Soltan-Panahi, J. Struck, P. Hauke, A. Bick, W. Plenkers, G. Meineke, C. Becker, P. Windpassinger, M. Lewenstein, and K. Sengstock, Multi-component quantum gases in spin-dependent hexagonal lattices, Nat. Phys. **7**, 434 (2011).

[27] B. Yang, H. N. Dai, H. Sun, A. Reingruber, Z. S. Yuan, and J. W. Pan, Spin-dependent optical superlattice, Phys. Rev. A **96**, 011602(R) (2017).

[28] M. Mancini, G. Pagano, G. Cappellini, L. Livi, M. Rider, J. Catani, C. Sias, P. Zoller, M. Inguscio. M. Dalmonte, and L. Fallani, Observation of chiral edge states with neutral fermions in synthetic Hall ribbons, Science **349**, 1510 (2015).

[29] B. K. Stuhl, H.-I. Lu, L. M. Aycock, D. Genkina, and I. B. Spielman, Visualizing edge states with an atomic Bose gas in the quantum Hall regime, Science **349**, 1514 (2015).

[30] L. Wang, M. Troyer, and X. Dai, Topological Charge Pumping in a One-Dimensional Optical Lattice, Phys. Rev. Lett. **111**, 026802 (2013).

[31] D. Culcer, Y. Yao, and Q. Niu, Coherent wave-packet evolution in coupled bands, Phys. Rev. B **72**, 085110 (2005).

[32] M. C. Chang and Q. Niu, Berry curvature, orbital moment, and effective quantum theory of electrons in electromagnetic fields, J. Phys.: Condens. Matter **20**, 193202 (2008).

[33] M. V. Berry, Quantal phase factors accompanying adiabatic changes, Proc. R. Soc. London A **392**, 45 (1984).

[34] F. Wilczek and A. Zee, Appearance of Gauge Structure in Simple Dynamical Systems, Phys. Rev. Lett. **52**, 2111 (1984).

[35] M. C. Chang and Q. Niu, Berry phase, hyperorbits, and the Hofstadter spectrum: Semiclassical dynamics in magnetic Bloch bands, Phys. Rev. B **53**, 7010 (1996).

[36] G. Sundaram and Q. Niu, Wave-packet dynamics in slowly perturbed crystals: Gradient corrections and Berry-phase effects, Phys. Rev. B **59**, 14915 (1999).

[37] D. Xiao, M. C. Chang, and Q. Niu, Berry phase effects on electronic properties, Rev. Mod. Phys. **82**, 1959 (2010).

[38] S. L. Zhang and Q. Zhou, Two-leg Su-Schrieffer-Heeger chain with glide reflection symmetry, Phys. Rev. A **95**, 061601(R) (2017).

[39] S. Xu and C. Wu, Space-Time Crystal and Space-Time Group, Phys. Rev. Lett. **120**, 096401 (2018).

[40] A. A. Soluyanov and D. Vanderbilt, Wannier representation of Z_2 topological insulators, Phys. Rev. B **83**, 035108 (2011).

[41] F. Grusdt, D. Abanin, and E. Demler, Measuring Z_2 topological invariants in optical lattices using interferometry, Phys. Rev. A **89**, 043621 (2014).

[42] A. Alexandradinata, Xi Dai, and B. A. Bernevig, Wilson-loop characterization of inversion-symmetric topological insulators, Phys. Rev. B **89**, 155114 (2014).

[43] T. Li, L. Duca, M. Reitter, F. Grusdt, E. Demler, M. Endres, M. Schleier-Smith, I. Bloch, and U. Schneide, Bloch state tomography using Wilson lines, Science **352**, 1094 (2016).

[44] T. Bzdušek and Manfred Sigrist, Robust doubly charged nodal lines and nodal surfaces in centrosymmetric systems, Phys. Rev. B **96**, 155105 (2017).

[45] L. Lu, C. Fang, L. Fu, S. G. Johnson, J. D. Joannopoulos, and M. Soljačić, Symmetry-protected topological photonic crystal in three dimensions, Nat. Phys. **12**, 337 (2016).

[46] T. Morimoto, H. C. Po, and A. Vishwanath, Floquet topological phases protected by time glide symmetry, Phys. Rev. B **95**, 195155 (2017).

[47] Y. Peng and Gil Refael, Floquet Second-Order Topological Insulators from Nonsymmorphic Space-Time Symmetries, Phys. Rev. Lett. **123**, 016806 (2019).

[48] M. Nakagawa, R.-J. Slager, S. Higashikawa, and T. Oka, Wannier representation of Floquet topological states, Phys. Rev. B **101**, 075108 (2020).